THE ASTROPHYSICAL JOURNAL, 374:744–752, 1991 June 20

X-RAY TO INFRARED OBSERVATIONS OF THE AM HERCULIS SYSTEM E1405−451 (V834 CENTAURI)[1]

R. M. SAMBRUNA,[2] L. CHIAPPETTI,[3] A. TREVES,[2] J. M. BONNET-BIDAUD,[4] P. BOUCHET,[5]
L. MARASCHI,[2] C. MOTCH,[6] AND M. MOUCHET[7]

Received 1990 June 19; accepted 1990 November 28

ABSTRACT

E1405−451 was observed in the X-ray band with the *EXOSAT* satellite in 1984 March during a high state. Simultaneous UV, optical, and IR coverage was obtained with *IUE* and from ESO telescopes. The source was detected both in the low energy (LE; 0.02–2.5 keV) and in the medium energy (ME; 1–20 keV) experiment on board *EXOSAT*. It is not possible to fit both bands with a single spectral law and single column density. The ME data are fitted by a bremsstrahlung spectrum of temperature $\gtrsim 1$ keV and hydrogen column density $N_{\rm H} \simeq 3 \simeq 10^{23}$ cm^{-2}. The LE emission may be described by a blackbody distribution. Taking into account also the UV observations the relevant parameters can be well determined with the result that $kT = 14$–15 eV and $N_{\rm H} = 5$–6×10^{19} cm^{-2}. The low-energy X-ray light curve shows a minimum at phase zero similar to the optical one, with some indication of temperature modulation with orbital phase. On the contrary, the medium energy X-ray light curve has a broad maximum at phase 0; the column density varies with phase which may account for the entire modulation of the intensity. The results are compared with the models of AM Her–like objects.

Subject headings: stars: binaries — stars: individual (V834 Centauri) — ultraviolet: spectra — X-rays: binaries

1. INTRODUCTION

The AM Her–type system E1405−451 was discovered in the X-ray band with the *HEAO 1* and *Einstein* satellites (Jensen, Nousek, & Nugent 1982) and identified with a 15th magnitude star by Mason et al. (1982). The classification as an AM Her system was proposed on the basis of the optical light curve, which shows modulation at a period of 101.5 minutes accompanied by rapid flickering. Observation of strong linear and circular polarization of the optical light confirmed the proposed classification (Tapia 1982; Bailey et al. 1983). All orbital phases calculated in this paper refer to the photometric ephemeris $T = \text{HJD } 2{,}445{,}048.9423476(45) + N \times 0.070497235(56)$ (Cropper, Menzies, & Tapia 1986), where $\phi = 0.0$ is at the center of the minimum of the optical light curve.

The optical and UV line spectra (Mason et al. 1983; Maraschi et al. 1984a; Rosen, Mason, & Cordova 1987; Takalo & Nousek 1988) are typical of the AM Her–type objects. They show strong emission lines (Balmer series, He II λ4686, C IV λ1550, Si IV λ1400).

E1405−451 exhibits high and low states (Maraschi et al. 1984a; Beuermann & Thomas 1989; Mason et al. 1989) similar to other AM Her systems. From observations of the Zeeman components of Hα and Hβ in the low state of early 1989, Beuermann et al. (1990) and Puchnarewicz et al. (1990) estimated the magnetic field to be $\sim(22 \pm 2) \times 10^6$ G, somewhat larger but not inconsistent with the value of 10–15×10^6 G, derived by Maraschi et al. (1984a) from data referring to the low state of 1983 March.

On the basis of polarization measurements, Cropper et al. (1986) give $i = 38° \pm 10°$, $\beta = 27° \pm 10°$ for the system inclination and magnetic colatitude, respectively. The 99% confidence values of i and β agree with those found by Beuermann et al. (1990) from the orbital motion of the cyclotron lines ($i \sim 50°$, $\beta \sim 40°$), and with those derived by Ferrario & Wickramasinghe (1990) from fits of the optical intensity and polarization curves with cyclotron models ($i = 45°$, $\beta = 15°$).

Spectral features in the red indicate that the companion star is a late M dwarf. Scaling the flux of the companion star to that of the template M star GL 406, Puchnarewicz et al. (1990) obtain $d \simeq 55$ pc. However, the same authors find $d \geq 70$ pc, using the method of Bailey (1981). In the following we assume $d \simeq 100$ pc.

E1405−451 was observed 3 times by the *EXOSAT* satellite in 1984 March, 1985 August, and 1986 March. In this paper we present the *EXOSAT* data of 1984 March together with the simultaneous UV data taken with *IUE* satellite and optical-IR photometry obtained at ESO. Preliminary reports were given by Maraschi et al. (1984b), Bonnet-Bidaud et al. (1985), Osborne, Cropper, & Cristiani (1987), and Osborne (1988). The observations of 1985 and 1986 will be discussed in detail in a forthcoming paper (Osborne et al., in preparation).

The paper is structured as follows. X-ray observations are described in § 2.1; results obtained from temporal and spectral analysis of these data are given in §§ 2.2 and 2.3, respectively. Phase variability of the spectral parameters is described in § 2.4; UV data are reported in § 3. The combination of UV and X-ray data is used in § 4 to restrict the uncertainties on the hydrogen column density and temperature. Optical and infrared light curves are examined in § 5.1, while in § 5.2 a cross-correlation between the X-ray and optical-IR data is considered. The results are discussed in § 6, focusing on the

[1] Based on data obtained with the *EXOSAT* and *IUE* satellites and ESO telescopes.

[2] Sezione di Astrofisica, Dipartimento di Fisica, dell' Università, via Celoria 16, 20133 Milano, Italy.
[3] Istituto di Fisica Cosmica e Tecnologie Relative del CNR, via Celoria 16, 20133 Milano, Italy.
[4] Dph SAP, CEN-Saclay, 91191 Gif-sur-Yvette, France.
[5] La Silla Observatory, la Serena, Chile.
[6] Observatoire de Besançon, 41 bis Av. de l'Observatoire, F-2544 Besançon Cedex, France.
[7] Observatoire de Paris-Meudon, 5 Place J. Jannsen, 92195 Meudon, France.

X-ray and optical energy distribution and the X-ray light curves. A summary and conclusions are reported in § 7.

2. X-RAY DATA

2.1. *Observations*

We use data from two of the instruments on board the *EXOSAT* satellite. The low energy imaging telescope (the LE experiment) operates in the soft X-ray band (0.02–2.5 keV). A photon-counting Channel Multiplier Array, without intrinsic energy resolution, was located in the focal plane. Five filters, interposed in the beam, offered broad-band spectral information.

The medium energy (ME) experiment consisted of eight argon-filled proportional counters sensitive in the 1–20 keV energy range. They were grouped to form two panels (halves). During the observations, one half was pointing toward the source (aligned half),[8] while the other monitored the sky ("offset half"), giving an independent background estimate. For a detailed description of the experiments see White & Peacock (1988) and references therein.

The journal of observations of E1405−451 is given in Table 1A. The LE data were taken with different filters: 3000 Å (thin) Lexan, aluminum-parylene, and 4000 Å (thick) Lexan (hereafter, 3000LX, Al-P, and 4000LX, respectively). Effective areas versus energy for the various filters are given in White & Peacock (1988). We evaluated the count rates in a box of optimum size of 50 pixels (1 pixel = 4″) centered on the source position. The background was estimated in a surrounding rectangular region. The mean source intensity in the three filters corrected for dead time, vignetting, background disuniformity, and point spread function is listed in Table 1A, together with exposure times.

The ME net light curve and spectrum were obtained from data taken in the *HER4* spectral mode (accumulation time 10 s). We subtracted the background measured simultaneously in the offset half and applied a correction for the intrinsic difference of the two halves, using the slew data. The signal was detected in the 2–9 keV energy range with a mean source intensity of 0.999 ± 0.076 counts s^{-1} $half^{-1}$. In the 1–3 keV interval a weak signal is present (0.328 ± 0.053 counts s^{-1} $half^{-1}$), but the background fluctuations are strong. Because of these uncertainties, these data were excluded from the analysis. We checked, however, that they are consistent with the results of spectral fits.

High temporal resolution data, obtained using the *HER5* timing mode (accumulation time 125 ms), taken simultaneously with the *HER4* mode data (see above), enable us to perform a short time-scale variability study (see § 2.2.3).

2.2. *Temporal Analysis*

2.2.1. *LE Experiment*

The LE net light curves are shown in Figure 1. Two narrow total eclipses appear at constant phases in each filter; the

[8] All count rates given in the text and figures refer to the on-source half experiment; this is indicated by the notation counts s^{-1} $half^{-1}$.

TABLE 1

JOURNAL OF OBSERVATIONS

A. X-RAY OBSERVATIONS

Instrument	Start Date (UT)	Start Time (UT)	End Time (UT)	Phase of Start Time	Exposure Time (s)	Count Rate (counts s^{-1})
LE + 3000LX	1984 Mar 24	02:07	05:10	0.97	9617	0.6972 ± 0.0089
LE + Al/P		05:14	07:38	0.81	3878	0.0450 ± 0.0041
LE + 4000LX		07:43	10:01	0.28	6818	0.5723 ± 0.0100
ME		01:46	10:03	0.76	29590	0.9990 ± 0.0760[a]

B. UV OBSERVATIONS

Camera/Image Number	Start Date (UT)	Start Time (UT)	End Time (UT)	Phase of Start Time	Exposure (s)
SWP 22570	1984 Mar 24	03:32	05:13	0.80	6060
LWP 03017		05:18	06:59	0.85	6060
SWP 22571		07:03	08:44	0.88	6060
LWP 03018		08:49	10:30	0.93	6060

C. OPTICAL AND IR OBSERVATIONS

Instrument	Wave band	Start Date (UT)	Start Time (UT)	End Time (UT)	Phase of Start Time	Integration time (s)
Danish 1.54 m	*B*(440 nm)	1984 Mar 23	6:03	8:22	0.11	20
Double channel	*V*(550 nm)		6:03	8:22	0.11	20
Photometer	*I*(790 nm)		6:05	8:26	0.13	20
ESO 3.6 m	*J*(1250 nm)	1984 Mar 23	5:14	9:27	0.63	30
InSb detector	*H*(1650 nm)		5:16	9:28	0.65	30
	K(2200 nm)		5:18	9:29	0.67	30
Danish 1.54 m	*V*(550 nm)	1984 Mar 24	4:55	9:30	0.62	0.1
ESO 3.6 m	*J*(1250 nm)		4:09	9:44	0.17	30

[a] Counts s^{-1} $half^{-1}$ in the range 2–9 keV.

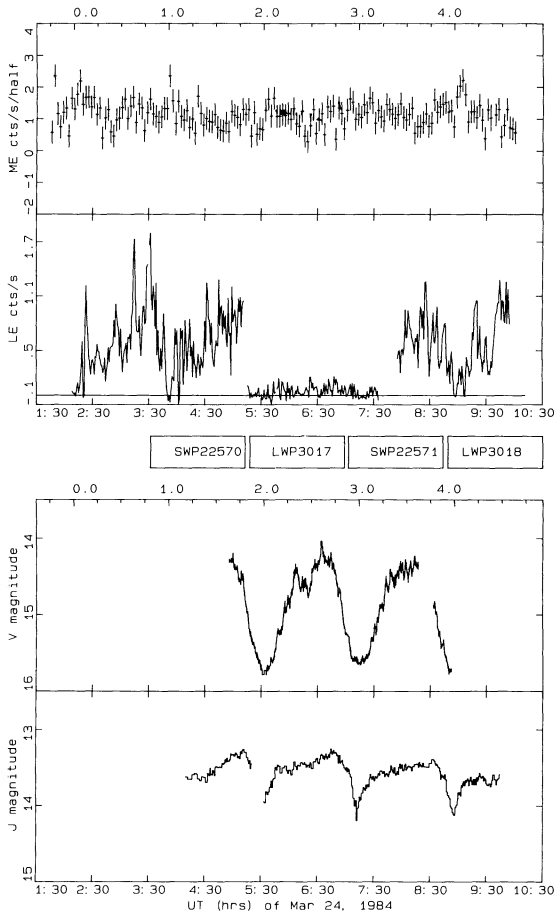

FIG. 1.—Light curves of E1405−451, taken on 1984 March 24, in the X-ray and optical-IR bands. From top to bottom: ME light curve in the energy range (2–9) keV (binned at 180 s); LE light curves (binned at 60 s) in the three filters (see Table 1); *V* light curve binned at 12.8 s; *J* light curve binned at 30 s. Boxes between the LE and *V* light curves indicate the UV coverage. Top axis of each frame is labeled in phase.

widths are comparable with the bin size (60 s). One eclipse (primary) occurs at optical phase $\phi = 0.0$, while the second one at $\phi = 0.1$.

The 3000LX light curve was Fourier analyzed using the Ferraz-Mello (1981) method. The only significant peak in the periodogram is the one corresponding to the optical period, whose significance corresponds to a chance probability $\leq 10^{-6}$. The optical period peak appears also in the Fourier analysis of the Al/P and 4000LX filters with chance probabilities $\leq 10^{-2}$ and $\leq 10^{-5}$, respectively. Note, however, the limited phase coverage with these filters.

Folded light curves (25 phase bins) are shown in Figure 2. Because of the chosen bin size the eclipses are scarcely visible in the folded curves. It is apparent that the general pattern of the folded light curves is similar for the three filters. There are appreciable differences between the 3000LX and 4000LX light curves; since the two filters differ only in thickness, this cannot be because of a spectral effect but is indicative of cycle-to-cycle (non–phase dependent) variability.

In order to study the shape of the light curves in the various filters, they were smoothed and folded; the percent deviations from the mean are displayed in Figure 3. A sawtooth pattern, with three bumps preceding the eclipses, is apparent in all filters. The bumps are not exactly at the same phase. The duty cycle of the bumps is $\Delta\phi \simeq 0.15$.

2.2.2. *ME Experiment*

The ME net light curve obtained as described in § 2.1 is plotted in Figure 1. Its periodogram shows a peak at the orbital period with a chance probability of 5.7×10^{-4}. The light curve of Figure 1 folded at the orbital period is plotted in Figure 2. The most remarkable feature is the broad maximum near $\phi \sim 0.0$, where the LE light curve has a minimum.

We define the pulsed fraction as the ratio of the area of the pulsed part of the light curve (i.e., above the minimum) to the total area under the light curve. With this definition, the pulsed fraction of the ME light curves is ~38%, compared to 100% in the LE light curves.

2.2.3. *Quasi-Periodic Oscillations*

Quasi-periodic oscillations (QPOs) of period ~2 s and coherence time ~1 minute were found in the optical band (Mason et al. 1983; Larsson 1985, 1987). In order to search for QPOs in the X-ray emission we analyzed both the LE and ME high–temporal resolution data. In the case of the ME experiment, we consider the *HER5* data (bin size 0.125 s) in the energy range 3–5 keV where most of the signal is present. For the LE data, the minimum bin size used is 1 s, dictated by the S/N ratio. The periodograms did not show any peak more significant than those found in the background.

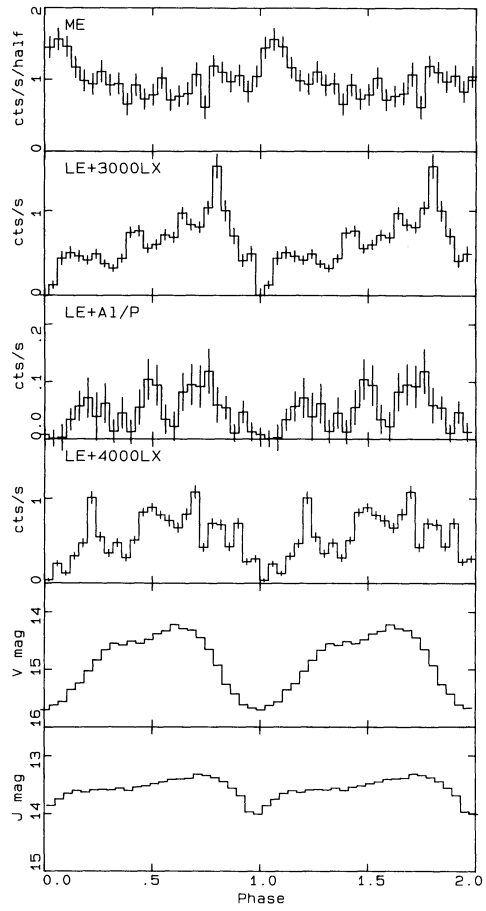

FIG. 2.—Light curves in the X-ray and optical-IR bands (see Fig. 1), folded according to the ephemeris of Cropper et al. (1986), using 25 phase bins.

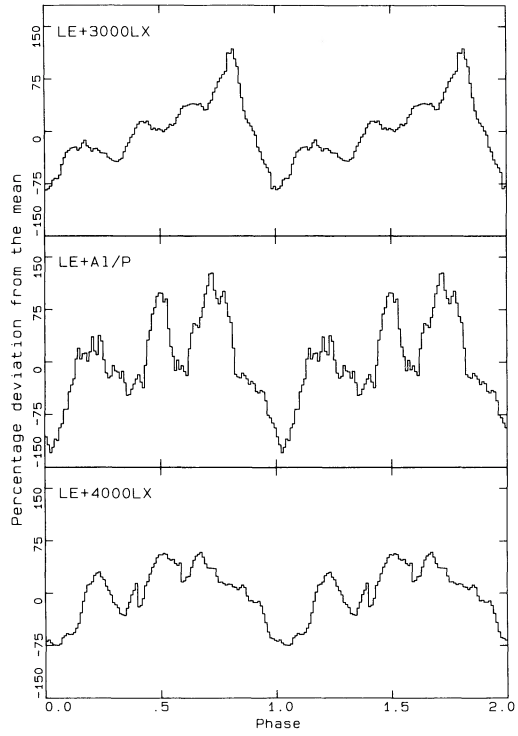

FIG. 3.—LE light curves smoothed with an 11 bin sliding mean and folded on the period. In order to allow an easier comparison, the percentage deviation from the mean value in each filter is shown.

2.3. *Spectral Analysis*

2.3.1. *LE Spectral Information*

Some spectral information can be derived from the LE data with the following method. If a given spectral distribution is assumed, and two interesting parameters are considered, one can compute the predicted ratio of count rates in two filters (e.g., Al/P and 3000LX) at any point of the parameter space. The locus of the points where the ratio is equal to the observed one can be plotted. Taking into account the errors on the count rates, one can plot a band where the ratio is within the observed range. The ranges allowed for the interesting parameters are found by projecting the intersection of the allowed regions onto the coordinate axes. The values of the remaining parameter(s) (usually the normalization) are determined in each point matching the predicted count rates in any of the filters with the observed one.

With the use of the procedure described above, we studied first the count rates averaged over the whole observation; we assumed a blackbody spectral law (in agreement with the standard model of AM Her systems; see, e.g., Liebert & Stockman 1985), with the temperature kT (eV) and the absorption column density $N_{\rm H}$ (cm^{-2}) as interesting parameters. The uncertainty bands in the $N_{\rm H} - kT$ plane were determined using 3 σ errors on the count rates. The results are displayed in Figure 4. The inferred parameters ranges (see region 2 of the figure) are $3 \leq kT \leq 17$ eV and $10^{19} \leq N_{\rm H} \leq 10^{21}$ cm^{-2}.

The hydrogen column density is poorly determined by the above procedure. Further constraints can be derived taking into account our UV observations (see § 4) which leads to the definition of region 6 in Figure 4. Reading off the graph, one has $N_{\rm H} \approx 5 \times 10^{19}$ cm^{-2} and $kT = 15 \pm 1$ eV. For these spectral parameters the total flux of the blackbody component, corrected for absorption, is estimated to be $\sim 3.4 \times 10^{-10}$ ergs cm^{-1} s^{-1}.

2.3.2. *ME Spectrum*

To fit the net spectrum averaged over the entire observation, the data were rebinned so that in each new bin the signal is at least at the 3 σ level. The results of fits with a bremsstrahlung distribution (in agreement with the standard model of the AM Her objects) and a power law (for comparison) are listed in Table 2A for the average spectrum. Best-fit parameter values and 90% confidence intervals are also given. The fit quality is similar for both spectral laws. This may derive from the limited statistical quality of the data. While the bremsstrahlung temperature and the photon index are poorly determined, the constraints on the column density of the medium energy X-ray emission give a value which is greater than previously found for the soft X-ray component by at least two orders of magnitude.

The two spectral components are illustrated in Figure 5. We attempted a joint fit (adding the observations in the LE filters, considered as independent channels, to the ME bins) with a bremsstrahlung or power law. This shows (not surprisingly) that these models cannot adequately describe the total spectrum and confirms that two distinct components are indeed present, the soft one described by a blackbody $kT \simeq 15$ eV (see § 2.3.1), the other one by a bremsstrahlung ($kT \simeq 3.5$ keV).

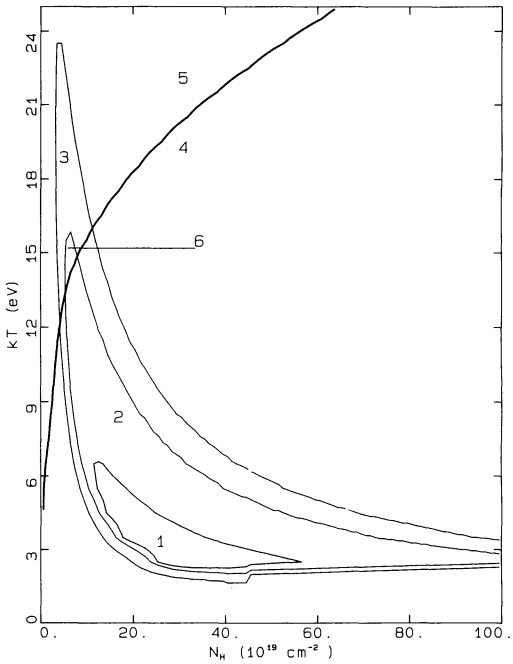

FIG. 4.—Determination of the parameters of the soft X-ray blackbody. The various regions are labeled as explained below. From the X-ray (LE filter ratio) data we can construct three regions: (1): hole inside region 2—allowed only by 4000LX over Al/P ratio, but excluded by 3000LX over Al/P ratio; (2) "good" region—allowed by both the 3000LX over Al/P and the 4000LX over Al/P ratios; (3) strip around region 2—allowed by the 3000LX over Al/P ratio, but excluded by the 4000LX over Al/P ratio. From the UV measurements we can divide the plane in two regions: (4) the one below the thick curve is excluded since the flux predicted by the soft X-ray blackbody at 1300 Å exceeds the measured value of 2.9×10^{-14} ergs cm^{-2} s^{-1} Å^{-1}; (5) the one above is allowed by UV measurements. The intersection of regions 2 and 5 is region 6, which is allowed by both X-ray and UV measurements.

TABLE 2

SUMMARY OF SPECTRAL FITS

A. X-RAY (ME)

Model	kT (keV)	Photon Index	N_H (10^{23} cm^{-2})	Flux at Source[a] (10^{-11} ergs cm^{-2} s^{-1})	χ^2	D.o.F.
Average Spectrum						
Bremsstrahlung:						
Best fit	3.5	...	3.0	4.7	4.9	9
90% range	>0.9	...	2.2–7.0	3.0–27	...	...
Power law:						
Best fit	...	3.7	4.0	8.7	4.9	9
90% range	...	>0.2	>1.0	1.8–12.8	...	...
"High Phase" Spectrum ($0.9 < \phi < 1.2$)						
Bremsstrahlung:						
Best fit	9.0	...	1.7	3.14	6.8	11
90% range	>2.2	...	1.0–3.8	2.3–8.3	...	...
Power law:						
Best fit	...	1.5	1.4	2.6	6.7	11
90% range	...	0.0–5.0	0.0–4.5	1.4–18	...	...
"Low Phase" Spectrum ($0.2 < \phi < 0.9$)						
Bremsstrahlung:						
Best fit	4.3	...	3.4	4.3	3.9	7
90% range	>0.9	...	2.2–8.6	4.0–76	...	...
Power law:						
Best fit	...	3.0	3.5	7.2	4.0	7
90% range	...	0.0–11	0.0–12	1.9–32	...	...

B. ULTRAVIOLET (IUE)

Model	Wavelength Index	A_V	χ^2	D.o.F.
Power law:				
Best fit	1.54	0.10	219	19
90% range	1.45–1.70	0.02–0.25	...	...

[a] X-ray flux computed in the range 3–8 keV.

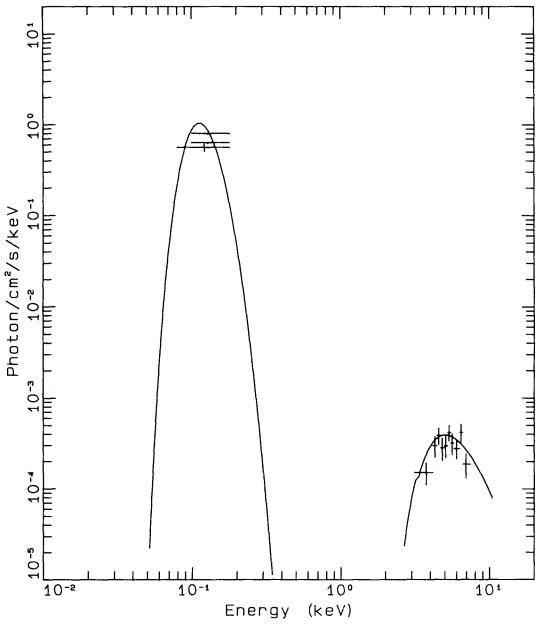

FIG. 5.—Composite X-ray photon spectrum at Earth, reconstructed using the LE blackbody ($T = 15$ eV, $N_H = 5 \times 10^{19}$ cm^{-2}) and ME bremsstrahlung ($T = 3.5$ keV, $N_H = 3 \times 10^{23}$ cm^{-2}) components.

2.4. *Phase Variability of X-Ray Spectra*

2.4.1. *Blackbody Component*

In order to study the possible phase dependence of blackbody parameters, LE count rates were derived from images accumulated in the following selected phase intervals: 0.0–0.25, 0.25–0.4, 0.4–0.6, 0.6–0.7, 0.7–0.9, and 0.9–1.0. The phase intervals were chosen by inspecting folded light curves (Figs. 2 and 3), so that in each phase interval the source intensity is approximately constant. The count rates in different filters were then studied with the method described in § 2.2.1.

A weak indication for temperature variability with orbital phase is inferred by comparing the allowed regions in the parameter space. If the N_H is fixed to the value ($N_H = 5 \times 10^{19}$ cm^{-2}) determined using the UV measurements (§ 4), one has $13 \leq kT \leq 30$ eV and $kT \leq 10$ eV in the 0.6–0.7 and 0.0–0.25 phase intervals, respectively.

2.4.2. *Thermal Component*

We accumulated ME phase-resolved spectra in the two phase intervals 0.9–1.2 and 0.2–0.9, corresponding to the high and low parts of the light curve. In the following we will refer to them as "high" and "low" phases.

Spectra were fitted with bremsstrahlung and power-law spectral forms; results are listed in Table 2A. Bremsstrahlung temperature or spectral index are both poorly determined,

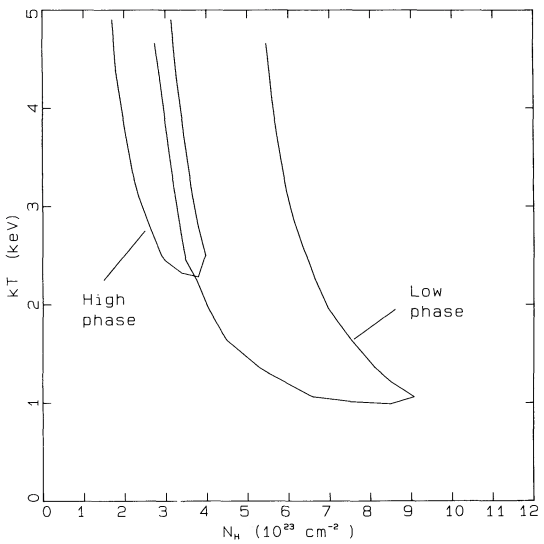

FIG. 6.—90% confidence contours in the $N_H - kT$ plane for the high- and low-phase spectra (see text), based on the best fit with a bremsstrahlung distortion.

although there is some indication of a steeper spectrum in the low phase (see Table 2A).

Absorption is better determined. In the high-phase interval it is a factor of 2 smaller than in the low-phase interval. This is shown in detail in Figure 6, where we plot the 90% confidence contours for both the low and high phases.

3. UV SPECTRUM

Low-resolution UV spectra of E1405−451 were obtained with *IUE* in the 1200–1980 and 1900–3200 Å bands (SWP and LWP cameras). The journal of observations is given in Table 1B. The UV observations cover almost exactly the same interval as the X-ray ones (see Fig. 1). The exposure times were chosen equal to the orbital period; thus, no phase-resolved study is possible. Spectra were reduced using the IUESIPS extraction and standard calibrations. No significant variability was found between the two LW and SW exposures, which therefore were summed. The resulting combined spectrum is reported in Figure 7.

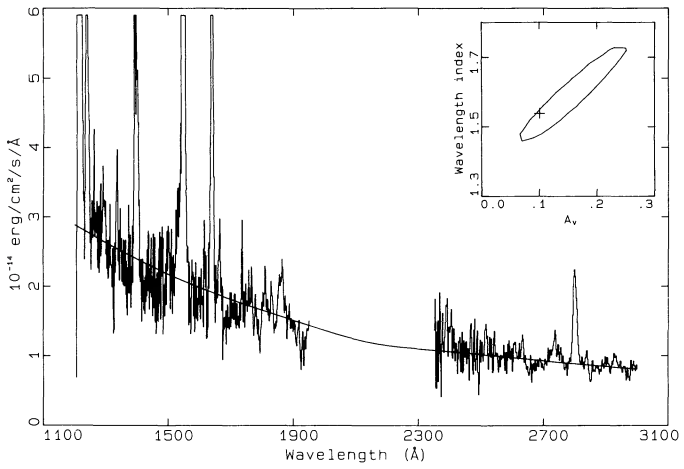

FIG. 7.—Average UV spectrum with the best-fit power law ($\alpha = 1.5$, $A_V = 0.1$). The inset shows the 90% confidence contour and the position of the best-fit values.

For the purpose of spectral fitting, continuum points were measured averaging the flux in intervals of 50 Å in selected regions free of lines. The statistical error in each interval was combined with a 10% systematic error. These data were best fitted with a power law, $F_\lambda \propto \lambda^{-\alpha_\lambda}$, reddened with the extinction curve of Seaton (1979). A standard χ^2 procedure was adopted. Best-fit values, 90% uncertainties, and minimum χ^2 are given in Table 2B. Contours in the $A_V - \alpha_\lambda$ plane corresponding to 90% uncertainty are displayed as an inset in Figure 7, yielding $0.03 \leq A_V \leq 0.25$. The value of A_V is compatible but somewhat lower than that given by Nousek & Pravdo (1983), $0.2 \leq A_V \leq 0.6$. Our UV spectrum is somewhat softer ($\alpha_\lambda = 1.5$) than that in Nousek & Pravdo (1983) and in Maraschi et al. (1984a), who both gave $\alpha_\lambda = 1.9 \pm 0.05$.

The UV spectrum is close in intensity and line features to the high states of 1983 February and April (Maraschi et al. 1984a). There is a clear difference with the low state of 1983 March, where the continuum was better fitted by a blackbody than by a power law and the lines were absent.

4. N_H, kT DETERMINATION AND COMPARISON WITH PREVIOUS X-RAY OBSERVATIONS

The blackbody emission can be further constrained combining the information from LE data with the UV ones, since the measured UV flux can be taken as an upper limit to the blackbody emission. Assuming $F(\lambda 1300) = 2.9 \times 10^{-14}$ ergs cm^{-2} s^{-1} Å^{-1} and $A_V = 0.1$ limits the allowed region in the $N_H - kT$ plane to lay above the thicker line shown in Figure 4. Combining with the constraints from the soft X-ray observations, one finds a rather restricted region for the temperature and the column density: $kT = 14$–15 eV, $N_H = 5$–6×10^{19} cm^{-2}.

These values of N_H are compatible with those deduced from the reddening at 90% confidence (see Table 2B), using a standard A_V/N_H relation (Bohlin 1975). One can also compare with the value obtained from the local distribution of hydrogen (Paresce 1984) in the direction and at the distance of the source, which yields, for $d = 100$ pc, $N_H = 5 \times 10^{19}$–1×10^{20} cm^{-2}. We conclude that the hydrogen column deduced from the soft X-ray data is compatible with being purely interstellar in origin. On the other hand, the hydrogen column from the hard X-ray observations $N_H \geq 10^{23}$ cm^{-2} is larger by at least two orders of magnitude and should be related to local absorption.

In order to compare our results with previous X-ray measurements, we computed the flux as in the *HEAO 1* A-2 LED band (0.18–0.48 keV) and the *Einstein* IPC band (0.2–4.0 keV) assuming a blackbody temperature $T = 15$ eV, a column density $N_H = 5 \times 10^{19}$ cm^{-2}, and the normalization corresponding to the flux measured by us. A comparison with the data reported by Jensen et al. (1982) shows that the state discussed here is weaker by a factor ~ 10 with respect to that of 1978 February measured by *HEAO 1*, and stronger by a factor of 2 with respect to the state of 1980 January measured by the *Einstein Observatory*.

5. OPTICAL PHOTOMETRY

5.1. *Observations*

Optical and infrared observations of E1405−451 were made at the European Southern Observatory on 1984 March, partly

simultaneously with the *EXOSAT* and *IUE* observations. The journal of the whole set of optical observations is reported in Table 1C. Photometric data were obtained in the *B*, *V*, and *I* Cousins bands (Bessell 1979) with the double-beam photometer attached to the Danish 1.54 m telescope and equipped with a RCA C31034A detector. A 9″ diaphragm was used. On March 23 consecutive 20 s *B*, *V*, and *I* integrations were made during 1.4 cycles through each filter. The observations were interrupted because of clouds. *U* measurements were also obtained before (phase 0.01) and after (phase 0.69) the monitoring of the source. The autoguider system was used for the long monitoring (~2.7 cycles) of the source in the *V* filter on March 24 with an integration time of 100 ms. During this night color measurements (including *U* filter) were obtained at phase 0.60.

Infrared observations were made at the 3.6 m telescope using an InSb detector and *J*, *H*, and *K* filters. Integrations of 30 s were obtained consecutively in each filter on March 23 during 2.4 cycles. Long monitoring in the *J* filter was done on March 24 during 3.3 cycles with a temporal resolution of 30 s.

5.2. *Optical and Infrared Light Curves*

5.2.1. *Orbital Light Curves*

Data obtained on 1984 March 23 are shown in Figure 8. A first description of these light curves was presented by Bonnet-Bidaud et al. (1985). The shape of the light curve changes with energy, showing a larger modulation and a broader minimum at short wavelengths. A secondary minimum most pronounced in the *V* filter is detected around phase 0.45. It was also present in some previously published light curves (Tuohy, Visvanathan, & Wickramasinghe 1985; Osborne et al. 1987), and it is described as a double-humped shape by Cropper et al. (1986).

Pulsed fractions for the *B*, *V*, *I*, *J*, *H*, and *K* filters, defined as in § 2.2.2, were computed from folded, orbital, 15-bin light curves and are found to be 35%, 56%, 53%, 29%, 21%, and 21%, respectively, in the different filters. Orbital mean values of the magnitudes are 15.5, 15, 14.2, 13.7, 13.4, and 13.1 in increasing wavelength order. The magnitude range in *V* (14.1–15.8) has about the same amplitude as observed by Tuohy et al. (1985) a few days later, but the mean level is brighter by 0.6 mag.

Infrared (*J*, *H*) light curves were previously published by Bailey et al. (1983). A comparison of their data with ours shows that the *J* light curves are similar in intensity and shape, while our *H* light curve is lower by about 0.4 mag with respect to theirs although the shape and amplitude are close. Such discrepancy was already pointed out by Maraschi et al. (1984a) and Cropper et al. (1986).

5.2.2. *Simultaneous X-Ray, Optical, and IR Fast Variability*

Figure 1 shows the fast photometric optical (*V*) and infrared (*J*) light curves obtained on March 24 simultaneously with X-rays. *V* data are binned in 12.8 s. Individual measurements are reported.

The shape of the infrared minima is slightly asymmetric with a steeper ingress. This is particulary pronounced for the second minimum. Besides the orbital modulation clearly present in both filters, differences are also observed from one cycle to the next one, particularly in the *V* light curve. The minimum of 0.3 mag present at 6:20 UT (around phase 0.45; see Fig. 1) is a short-term variable feature since it disappears in two consecutive cycles. It may be related to the strong flaring activity present in the high part of this cycle. The narrow minimum at phase 0.0 clearly seen in the *U* light curve obtained by Mason et al. (1983) and to a less extent in the *V* band is not detected in our high–temporal resolution *V* data. In particular, there is no counterpart to the sharp, soft X-ray eclipses.

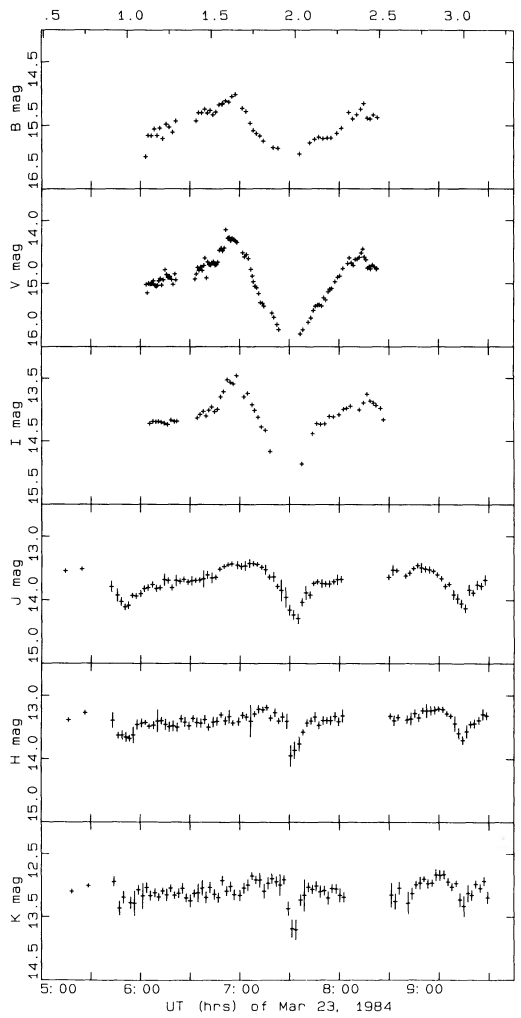

FIG. 8.—Light curves in the *B*, *V*, *I*, *J*, *H*, and *K* bands of 1984 March 23. Top frame axis is labeled in phase.

The large oscillations on a time scale of a few minutes detected in optical and in soft X-rays (see Fig. 1) were analyzed by cross-correlating simultaneous LE and *V* data in the part where this modulation is clearly present (from 7:55 to 8:15). No obvious correlation is found.

We have looked also for short quasi-periodic oscillations by constructing FFTs over consecutive 7 minute intervals across the *V* light curve. The 0.5 Hz excess in the power spectrum, first reported by Mason et al. (1983) and studied in detail by Larsson (1985, 1987), is clearly present outside the minima. It is variable in position (0.3–0.7 Hz), width (0.002–0.3 Hz), and intensity.

6. DISCUSSION

The "canonical" model of accretion onto magnetized phase-locked white dwarfs (e.g., Lamb 1985; Liebert & Stickman 1985) represents a well-established general framework for the understanding of AM Her–type systems. On the other hand, significant deviations from that simple picture have been inferred from the large body of data presently available (e.g., Cropper 1988; Beuermann 1988).

In particular, for E1405−451, phase-resolved spectroscopy implies considerable structure within the accretion column (Rosen et al. 1987), and detailed modeling of the cyclotron light curves indicates that the cyclotron emission region is arclike with wide angular extent (Ferrario & Wickramasinghe 1990; Cropper 1989). The presence of a second active pole not diametrically opposed to the principal one has also been suggested (Cropper 1989). In the following, we discuss our results in the light of such models.

1. *Energy distribution in the optical-IR band.*—The simultaneous optical and infrared observations allow us to derive the broad-band energy distribution in such domain and to study its phase variability. In particular, it is interesting to evaluate the shape of the cyclotron component.

We first derived the observed energy distribution at phases 0.0 and 0.5, taking from the folded light curves the flux values in the *B*, *V*, *I*, *J*, *H*, and *K* bands closest to the chosen phases, consistently with the phase bin width of $\Delta\phi = 0.066$. The *U* flux was, instead, evaluated using a color index $U-B = 1.05$ at phase 0.0 and $U-B = 0.6$ at phase 0.5. These indexes were obtained from individual measurements done at phases 0.01, 0.60, and 0.69 before and after the long monitoring of March 23 and 24.

In order to derive the net cyclotron contribution we subtracted the emission of the secondary and of the white dwarf using the results of Puchnarewicz et al. (1990) obtained during a low state. The corrected fluxes, dereddened with $A_V = 0.1$ (see § 3), are plotted in Figure 9.

In Figure 9*a* our data are compared with the broad-band energy distribution predicted at the two phases from the constant temperature model of Wickramasinghe & Meggitt (1985). An inclination $i = 45°$, a magnetic colatitude $\beta = 40°$, a temperature $kT = 40$ keV, and cyclotron opacities $\Lambda_d = 10^4$, $\Lambda_h = 10^3$ were adopted. In Figure 9*b* the data are compared with the energy distribution obtained in the shock front model of Cropper et al. (1986, Fig. 14*b*), with $i = 37°$, $\beta = 20°$, and $kT = 20$ keV. A magnetic field value of 25×10^6 G is used (see Introduction).

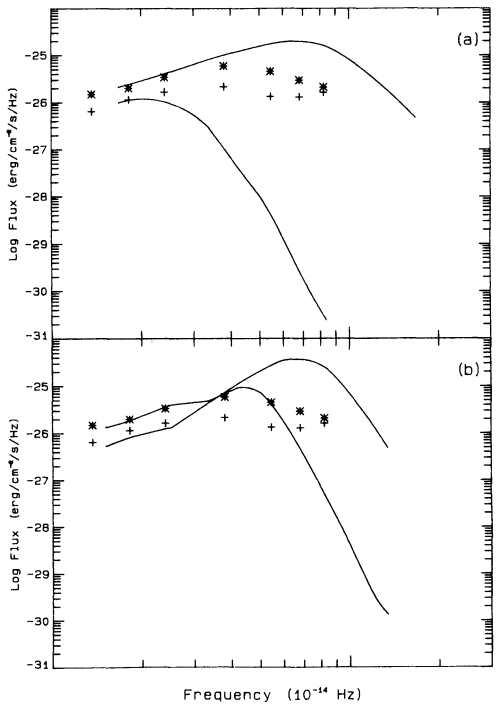

FIG. 9.—Comparison of our estimate of the cyclotron flux with literature best fits. The data shown in both panel for phase 0.0 (*crosses*) and phase 0.5 (*stars*) have been derived from our light curves in the *B*, *V*, *I*, *J*, *H*, and *K* bands, and from a single *U* measurement (see text for details). Solid curves represent the best fit at the two phases, as derived from the models of (*a*) Wickramasinghe & Meggitt 1985, and (*b*) Cropper et al. 1986. Curves have been arbitrarily scaled to match our measurements in the IR range (*H* and *K* bands).

While at longer wavelengths there is a reasonable agreement between the two models and the data, at shorter wavelengths both models fail to account for the residual energy distribution and for its phase dependence. The predicted slope of the optically thin cyclotron emission (at short wavelengths) is definitely too steep, and the predicted changes with phase too large. A possible way of resolving this discrepancy is to postulate the existence of an additional blue component largely exceeding the Rayleigh-Jeans tail of the soft X-ray blackbody. This may derive from thermal emission of the accretion stream, possibly near the stagnation region in the magnetosphere. It is also conceivable that more realistic models for the cyclotron radiation, involving wide and elongated emission regions (e.g., Ferrario & Wickramasinghe 1990) may lead to different prediction for the cyclotron energy distribution.

2. *X-ray spectral parameters and light curves.*—The existence of two components in the X-ray band is in agreement with the "canonical" model of accretion of the AM Her systems, which attributes the hard component to optically thin bremsstrahlung of shocked gas at the base of the column and the soft component to thermal radiation from the polar cap.

A further consistency with the canonical model is the fact that the radius of the region emitting the soft X-ray component, $R_{\rm soft} = 4.8 \times 10^7$ cm (derived from the normalization of the blackbody component), is found to be similar to that of the polar cap computed from the balance of magnetic and gas pressure, which, assuming $B = 20 \times 10^6$ G (see Introduction), turns out to be $r = 4.0 \times 10^7$ cm.

However, we encounter the well-known soft excess paradox pointed out by King & Lasota (1979, 1980). In our case the hard to soft X-ray luminosity ratio is in the range 0.1–1.0 (see Table 2A and § 2.3.1), while the predicted value is greater than or equal to 1.8. Although the universality of this phenomenon in AM Her objects is questionable (e.g., Beuermann, Stella, & Patterson 1987), we clearly include E1405−451 within the polars showing an excess of the soft X-ray emission. It is worth mentioning that a possible resolution of the paradox lies in a direct kinetic energy transport onto the surface from a filamentary accretion stream.

A remarkable result of our analysis is that the bremsstrahlung radiation is always seen through a relatively thick absorption column, while the X-ray blackbody is not. This suggests that the bremsstrahlung region is surrounded by absorbing walls, while the soft X-ray emission region is larger, and external to the foot of the absorbing walls. This configuration agrees with the inference by Beuermann et al. (1987) of a "cyclotron halo" surrounding the bremsstrahlung emission region. The absorbing walls could be identified with the boundary of the accretion column, where the stream should be thicker and cooler.

Our spectral analysis indicates that the ME light curve with its maximum at phase 0.0 can be understood as due to a reduced absorbing column at such phase. At this phase the line of sight makes the minimum angle to the accretion column;

thus, it is impossible to justify a reduced absorption depth at this phase if the accretion column is homogeneous. Again the concept of an inhomogeneous structured flow with high-density streams, which may be confined to the walls of the column, can reconcile the model with the observations. The concept of a hollow column is mentioned by Schmidt (1985).

Another important issue is the repeated eclipse of the soft X-ray emission near phase 0.0. These must be due to the accreting gas further above the column, where the stream bends over from the secondary. The same explanation is proposed by Rosen et al. (1987). An absorption depth of 10^{21} cm^{-2} is sufficient to absorb the soft X-ray, and a large area can be occulted. Again, substructures in the accretion flow may explain why the eclipse is double.

7. SUMMARY AND CONCLUSIONS

Our observations of E1405−451 show significant departures from the canonical model of AM Her–type objects in the following ways:

1. The infrared to optical energy distribution substantially exceeds at high frequencies the predictions from cyclotron models.

2. The luminosity in the soft X-ray blackbody component is definitely larger than that of the bremsstrahlung component at medium X-ray energies.

3. The absorbing column towards the harder X-ray component is at all phases much larger than that toward the soft X-ray component.

4. The absorbing column is minimum at phase 0.0 for the medium energy X-rays.

5. The soft X-ray component undergoes two total narrow eclipses near phase 0.0.

These features can be understood if the idealized model of a homogeneous accretion column is abandoned. The flow should be denser along the walls of the column, and the bremsstrahlung emission should occur within such walls, while the soft X-rays derive from a larger area surrounding the base of the accretion column.

We are grateful to J. P. Osborne for his contribution to a preliminary analysis of the data.

REFERENCES

Bailey, J. 1981, MNRAS, 197, 31
Bailey, J., Axon, D. J., Hough, J. H., Watts, D. J., Giles, A. B., & Greenhill, J. G. 1983, MNRAS, 205, 1P
Bessell, M. S. 1979, PASP, 91, 589
Beuermann, K. 1988, Adv. Space Res., 8, 283
Beuermann, K., Schwope, A. D., Thomas, H.-C., & Jordan, S. 1990, in Proc. 11th North American Workshop on CVs and LMXRBs, ed. C. W. Mauche (Cambridge: Cambridge University Press), in press
Beuermann, K., Stella, L., & Patterson, J. 1987, ApJ, 316, 360
Beuermann, K., & Thomas, H.-C. 1989, IAU Circ., No. 4775
Bohlin, R. 1975, ApJ, 200, 402
Bonnet-Bidaud, J. M., et al. 1985, in Recent Results on Cataclysmic Variables (ESA SP-236, June 1985), 155
Cropper, M. 1988, Adv. Space Res., 8, 273
———. 1989, MNRAS, 236, 935
Cropper, M., Menzies, J. W., & Tapia, S. 1986, MNRAS, 218, 201
Ferrario, L., & Wickramasinghe, D. T. 1990, ApJ, 357, 582
Ferraz-Mello, S. 1981, AJ, 86, 619
Jensen, K. A., Nousek, J. A., & Nugent, J. J. 1982, ApJ, 261, 625
King, A. R., & Lasota, J. P. 1979, MNRAS, 188, 653
———. 1980, MNRAS, 191, 721
Lamb, D. Q. 1985, in Cataclysmic Variables and Low-Mass X-ray Binaries, ed. D. Q. Lamb & J. Patterson (Dordrecht: Reidel), 179
Larsson, S. 1985, A&A, 145, L1
Larsson, S. 1987, Ap&SS, 130, 187
Liebert, J., & Stockman, H. S. 1985, in Cataclysmic Variables and Low-Mass X-ray Binaries, ed. D. Q. Lamb & J. Patterson (Dordrecht: Reidel), 151
Maraschi, L., et al. 1984a, ApJ, 285, 214
———. 1984b, in Proc. 4th *IUE* Conf. (ESA SP-218), 427
Mason, K., et al. 1982, IAU Circ., No. 3684
———. 1983, ApJ, 264, 575
———. 1989, IAU Circ., No. 4717
Nousek, J. A., & Pravdo, S. H. 1983, ApJ, 266, L39
Osborne, J. P., Cropper, M., & Cristiani, S. 1987, Ap&SS, 131, 643
Osborne, J. P. 1988, Mem. Soc. Astr. Italiana, 59, 117
Paresce, F. 1984, AJ, 96, 1022
Puchnarewicz, E. M., Mason, K. O., Murdin, P. G., & Wickramasinghe, D. T. 1990, MNRAS, 244, 20P
Rosen, S. R., Mason, K. O., & Cordova, F. A. 1987, MNRAS, 224, 987
Schmidt, G. D. 1985, in Cataclysmic Variables and Low Mass X-ray Binaries, ed. D. Q. Lamb & J. Patterson (Dordrecht: Reidel), 219
Seaton, M. J. 1979, MNRAS, 187, 73P
Takalo, L. O., & Nousek, J. A. 1988, ApJ, 327, 328
Tapia, S. 1982, IAU Circ., No. 3685
Tuohy, I. R., Visvanathan, N., & Wickramasinghe, D. T. 1985, Ap&SS, 118, 291
White, N. E., & Peacock, A. 1988, Mem. Soc. Astr. Italiana, 8, 7
Wickramasinghe, D. T., & Meggitt, S. M. A. 1985, MNRAS, 216, 857